ADVANCED FUNCTIONAL MATERIALS
www.afm-journal.de

Counterion Control and the Spectral Signatures of Polarons, Coupled Polarons, and Bipolarons in Doped P3HT Films

Eric C. Wu, Charlene Z. Salamat, Omar León Ruiz, Thomas Qu, Alexis Kim, Sarah H. Tolbert, and Benjamin J. Schwartz**

When an electron is removed from a conjugated polymer, such as poly(3-hexylthiophene-2,5-diyl) (P3HT), the remaining hole and associated change in the polymer backbone structure from aromatic to quinoidal are referred to as a polaron. Bipolarons are created by removing the unpaired electron from an already-oxidized polymer segment. In electrochemically-doped P3HT films, polarons, and bipolarons are readily observed, but in chemically-doped P3HT films, bipolarons rarely form. This is explained by studying the effects of counterion position on the formation of polarons, strongly coupled polarons, and bipolarons using both spectroscopic and X-ray diffraction experiments and time-dependent density functional theory calculations. The counterion positions control whether two polarons spin-pair to form a bipolaron or whether they strongly couple without spin-pairing are found. When two counterions lie close to the same polymer segment, bipolarons can form, with an absorption spectrum that is blueshifted from that of a single polaron. Otherwise, polarons at high concentrations do not spin-pair, but instead *J*-couple, leading to a redshifted absorption spectrum. The counterion location needed for bipolaron formation is accompanied by a loss of polymer crystallinity. These results explain the observed formation order of single polarons, coupled single polarons, and singlet bipolarons in electrochemically- and chemically-doped conjugated polymers.

1. Introduction

Semiconducting conjugated polymers, such as poly(3-hexylthiophene-2,5-diyl) (P3HT; see **Scheme 1**a for chemical structure), have found applications in flexible electronics, such as light-emitting diodes, photovoltaics, and thermoelectric devices.[1–5] To improve their performance in many of these applications, conjugated polymer films are often doped to introduce equilibrium charge carriers on the π-conjugated polymer backbone. Charge carrier creation in conjugated polymer films can be achieved through either electrochemical or chemical doping. In electrochemical doping, the conducting working electrode is coated with the conjugated polymer and a voltage is applied to create an electric potential difference between the electrodes.[6] The applied voltage causes electrons to be removed from (*p*-type) or added to (*n*-type) the conjugated π-system; counterions must then be incorporated into the polymer film to balance the charge.[7] In chemical doping, which is usually *p*-type,[8] a strong oxidizing agent, such as 2,3,5,6-tetrafluoro-7,7,8,8-tetracyanoquinodimethane (F_4TCNQ, see Scheme 1f for chemical structure) or iron (III) chloride ($FeCl_3$), is used to remove electrons from the polymer backbone.

When an electron is removed from the π-system of a conjugated polymer, such as P3HT, the backbone locally changes structure from aromatic to quinoidal, as depicted in Scheme 1b. The unpaired electron that remains, along with the accompanying distorted backbone structure, are together referred to as a polaron. In the traditional band picture borrowed from the language of inorganic semiconductors,[9–11] polaron creation causes two electronic energy levels that are associated with the half-filled state to move into the band gap, which creates two new allowed optical transitions, P1 and P2, shown in Scheme 1e. In most doped conjugated polymers, the lower-energy P1 transition usually occurs in the mid-infrared (mid-IR) near 0.5 eV, while the higher-energy P2 transition appears roughly an eV below the band gap, usually in the near-infrared (NIR).[12,13]

If the oxidative driving force to remove electrons is strong enough, an already-oxidized polymer segment can be oxidized again, removing the unpaired electron from the half-occupied level in the band gap. This removes the radical character on the polymer backbone, and the resulting doubly-charged species is referred to as a singlet bipolaron, depicted in Scheme 1c.[14] In the traditional band picture, this removal of a second electron causes the two intra-gap states to move further into the gap and away from the band edges, as shown in Scheme 1e.[9–11]

E. C. Wu, C. Z. Salamat, O. L. Ruiz, T. Qu, A. Kim, S. H. Tolbert, B. J. Schwartz
Department of Chemistry and Biochemistry
University of California, Los Angeles
Los Angeles, CA 90095-1569, USA
E-mail: tolbert@chem.ucla.edu; schwartz@chem.ucla.edu
S. H. Tolbert
Department of Materials Science and Engineering
University of California, Los Angeles
Los Angeles, CA 90095-1595, USA
The ORCID identification number(s) for the author(s) of this article can be found under https://doi.org/10.1002/adfm.202213652.

DOI: 10.1002/adfm.202213652

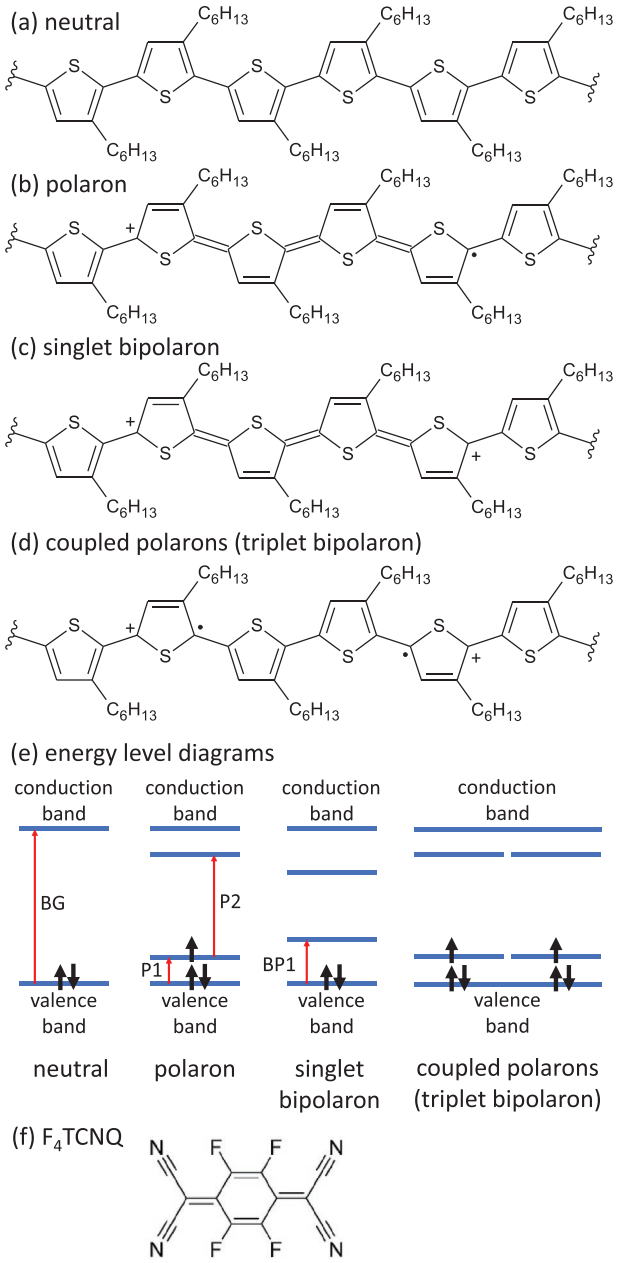

Scheme 1. Chemical structures of a) neutral P3HT, b) P3HT polaron, c) P3HT singlet bipolaron, and d) strongly-coupled polarons (triplet bipolaron) on P3HT. Panel e) shows traditional energy level diagrams for the different P3HT polaronic species. Panel f) shows the chemical structure of F_4TCNQ. A polaron (panel (b)) is a radical with a single positive charge, while a singlet bipolaron (panel (c)) is a doubly-charged species that is formally closed-shell. Well-separated polarons (panel (d)) can have open-shell character.

The resulting allowed bipolaronic optical transition, referred to as BP1, is bluer than the P1 transition of the single polaron and typically occurs between 0.8 and 1.1 eV; this transition has been observed in many highly-doped conjugated polymers, including poly(3,4-ethylenedioxythiophene) (PEDOT) and derivatives,[15–18] P3HT and derivatives,[19–22] as well as other conjugated polymers.[23–27]

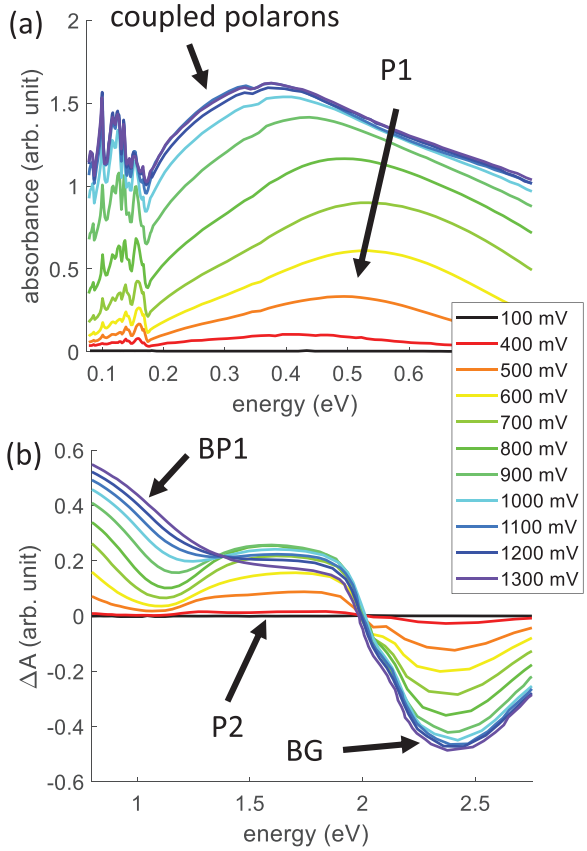

Figure 1. a) The absorption spectra and b) the difference spectra of the electrochemically-doped P3HT films as a function of applied potential relative to Ag/Ag^+. The data were taken from the work of Enengl et al. in Ref. [28]. Enengl et al. and Spano and co-workers[29] both have assigned the absorption peak near 0.3 eV that appears at high oxidation potentials as the absorption of singlet bipolarons. Throughout this work, however, we argue that this absorption feature arises from strongly-coupled polarons (triplet bipolarons), and that the blue shoulder seen near 1.0 eV is the absorption band associated with singlet bipolarons. We label the peaks in (a) and (b), accordingly.

Despite all this support for the way polarons and bipolarons behave in doped conjugated polymers, Enengl et al. recently have proposed a different picture.[28] As shown in **Figure 1**, these researchers monitored both the visible/NIR (panel b) and mid-infrared (panel a) absorption spectrum of P3HT films during electrochemical doping. When Enengl et al. increased the oxidative driving force to be high enough for bipolaron formation (≥800 mV vs. Ag/Ag^+), they saw the absorption band in the mid-IR region shift to the red, from ≈0.5 to ≈0.3 eV, as evident in Figure 1a. In combination with electron paramagnetic resonance (EPR) measurements, these workers concluded that the spectral redshift was caused by the formation of bipolarons.[28] This implies that the BP1 transition lies to the red of the P1 transition, which is contrary to the traditional band picture shown in Scheme 1e, where BP1 lies to the blue of P1. We note, however, that the data in Figure 1b also show the simultaneous growth of a new peak in the 0.8–1.0 eV region that creates the isosbestic point near 1.4 eV. Enengl et al. did not comment on this feature, which would be consistent with the BP1 transition in the traditional picture of bipolaron formation.

Intrigued by the conclusions of Enengl et al., Spano and coworkers took their previously presented model based on the Holstein Hamiltonian that successfully explains the mid-IR polaron absorption in P3HT[30–38] and extended it to describe bipolarons.[29] When they did this, their extended model predicted that the P3HT bipolaron spectrum should lie to the red of the single polaron spectrum, which appears to corroborate the conclusions of Enengl et al.[28] We note, however, that the Holstein Hamiltonian does not explicitly include any type of electron correlation and thus cannot account for spin when multiple particles are involved. This means that it is not clear if the model is correctly able to describe a spin-paired singlet bipolaron, or if it is better thought of as describing the behavior of two strongly-coupled single polarons without any definite spin relationship between them.

All of this leads to the main questions that we address in this paper: what are the electronic structure and spectral signatures of bipolarons in doped conjugated polymer films? Why do most experiments suggest that the BP1 absorption band lies to the blue of the P1 transition,[15–26] while the experiments in Figure 1[28] and the 2-particle Holstein model[29] suggest that BP1 lies to the red of P1? Why are bipolarons readily observed in electrochemically-doped films, but rarely observed in chemically-doped films?

Here, we answer these questions using spectroscopic and structural experiments in combination with time-dependent density functional theory (TD-DFT) calculations that employ a range-separated hybrid functional. We argue that it is the positions of the counterions in doped conjugated polymer films that control whether two close-lying polarons spin-pair to form a singlet bipolaron or instead retain their single-polaron/open-shell character while strongly perturbing each other. We show that if the counterions are located so that the singlet bipolaron is stabilized, the traditional picture holds and the BP1 transition appears to the blue of the P1 transition. For other arrangements of the counterions, however, two nearby polarons cannot stably spin pair, but the transition dipoles of their P1 absorptions, which lie along the polymer backbone, can strongly *J*-couple to produce a redshifted absorption. Thus, the redshifted absorption observed by Enengl et al.[28] and Spano and coworkers[29] are associated with strongly coupled single polarons and not with spin-paired bipolarons. In addition, we show that the positions of the counterions are related to the crystallinity of the polymer: bipolaron formation requires counterion positions that are not compatible with highly crystalline films. The fact that polaron interactions are controlled by the counterion positions also explains why bipolarons are much more commonly observed via electrochemical doping than via chemical doping: counterions are much more mobile in films that are swollen with the electrolyte solution in electrochemical doping. The spatial location of oxidizing equivalents and counterions is also quite different in chemical and electrochemical doping, leading to different counterion locations in each case.

2. Results and Discussion

2.1. TD-DFT Calculations of Polarons and Bipolarons on P3HT Oligomers

We begin our exploration of the electronic structure of polarons and bipolarons in doped conjugated polymer films by performing quantum chemistry calculations. As further described in the Experimental Section, we will take advantage of TD-DFT calculations using a range-separated hybrid functional, ωPBE, to understand the stability and spectroscopy of oxidized P3HT oligomers in the presence of counterions with a variety of positions relative to the chain backbone. We note that others also have investigated the idea that counterion positions make a difference in the electronic structure of P3HT polarons and bipolarons.[39–41] For example, Bendikov and co-workers[40,41] performed DFT calculations at the B3LYP/6-31G(d) level of theory and found that a singlet bipolaron configuration is preferred at high polaron concentrations, while a polaron pair configuration (triplet bipolaron) is preferred at low concentrations.[40] However, these workers concluded that even in the presence of counterions, singlet bipolarons are intrinsically unstable with respect to dissociation into polaron pairs,[41] a result that is not consistent with experiment. Zozoulenko and co-workers also studied counterion effects on doped P3HT, taking advantage of TD-DFT calculations with the B3LYP and ωB97XD functionals.[39] However, these workers did not distinguish between singlet and triplet bipolarons in their calculated spectra. Moreover, these workers placed the simulated counterions on top of the thiophene rings, but both experiments[42,43] and simulations[44] have shown that counterions prefer to sit in the lamellar region of the polymer crystallites, among the hexyl side chains rather than near the polymer π-system.

One of the issues when analyzing the results of DFT calculations on charged P3HT oligomers is that it is quite difficult to interpret the spin density (or any of the Kohn–Sham orbitals) as belonging to a particular energy level.[39,45] Thus, to best visualize the nature of the polarons and bipolarons in our calculations, we take advantage of the change in bond length associated with quinoidal nature of charged species on the P3HT backbone. The changes in bond length between a neutral P3HT oligomer with predominantly aromatic character and the same oligomer with charged (or doubly-charged) quinoidal character is depicted in **Figure 2**. As might be expected from the Lewis structures shown in Scheme 1, the C—C bonds that had more double-bond character on a neutral P3HT chain become longer and more single-bond-like while the bonds that had more single-bond character become shorter and more double-bond-like when the chain becomes charged. Since this change from aromatic to quinoid character only takes place in the presence of charges, the changes in the bond lengths provide a straightforward way to visualize the location of a polaron or bipolaron.[27] The absolute bond lengths of the neutral and charged P3HT oligomers are shown in Figure S2 (Supporting Information).

In addition to changes in bond lengths, another method that can be used to visualize the location and size of polarons or bipolarons is the change in the partial charges on the backbone C and S atoms of P3HT. Figure S1 (Supporting Information) shows how the Mulliken charges change as a P3HT chain goes from neutral to singly oxidized. The results are in excellent qualitative agreement with the changes in bond length shown in Figure 2, so that either the bond length or Mulliken charge changes can be used to visualize the location and spatial extent of polarons and bipolarons. For simplicity and ease of comparison to previous work,[27] we will focus on the changes in bond length in what follows.

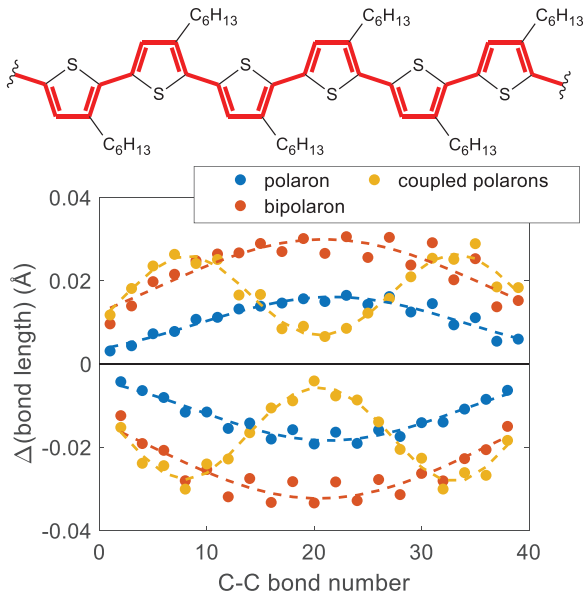

Figure 2. Differences in C—C bond lengths between the neutral and charged species for different charged states of a 10-mer of P3HT with no counterions, calculated at the PBE0/6-31G** level of theory. The bond length changes are shown for a single polaron (blue), coupled single polarons (triplet bipolaron; yellow) and singlet bipolaron (red). The dashed curves are fits of the bond length changes to Gaussian distributions to represent the position and extent of delocalization of the different charged species, as described in the Supporting Information.

The blue curves in Figure 2 show the calculated changes in bond length for a single polaron (without any counterions) on a P3HT 10-mer. The curves make it clear that the polaron resides in the center of the chain and is delocalized over roughly 5 monomer units, in excellent agreement with recent experimental measurements of the polaron coherence length.[43] The red curves in Figure 2 show the results for a singlet bipolaron on the same oligomer (again, without counterions). The bond length changes are slightly larger and the spatial width of the quinoid-like distortion are a bit larger than those of a single polaron, but otherwise a singlet bipolaron and a single polaron have a generally similar shape and spatial extent.

We also wanted to calculate the spatial distribution of two polarons that are not spin-paired. Since this is not possible with quantum chemistry, we instead have chosen to investigate triplet bipolarons as a proxy for polaron pairs that are not spin-paired (i.e., two single polarons that do not behave as a singlet bipolaron at high doping densities). The orange curves in Figure 2 show the changes in bond lengths for a triplet bipolaron on the same P3HT 10-mer (again, without counterions). In this case, the changes in bond length have a bimodal structure, with the two charges migrating toward opposite ends of the chain within the limit that their delocalization will allow. This is consistent with Scheme 1d, which shows that the chemical structure of a triplet bipolaron has aromatic thiophenes sandwiched between two segments of quinoid thiophenes associated with the two charges. Thus, the triplet bipolaron serves as a good proxy for two single polarons that are forced to interact without spin pairing at high doping densities.

Table 1. Binding energies of singlet bipolarons and strongly-coupled single polarons (triplet bipolarons) for 5-mer, 6-mer, and 10-mer P3HT chains with and without negative point charges at different positions along the backbone (Scheme 2).[a)]

	Binding Energy [eV]	
	Singlet Bipolaron	Coupled Polarons
5-mer (no point charges)	–1.40	–1.32
5-mer (3,3)	–0.47	–0.49
6-mer (no point charges)	–1.30	–0.98
6-mer (3.5,3.5)	–0.42	–0.24
10-mer (no point charges)	–1.27	–0.26
10-mer (5.5,5.5) $d = 5$Å[b)]	0.51	0.78
10-mer (5.5,5.5)	–0.35	0.22
10-mer (5,6)	–0.28	0.17
10-mer (4,7)	–0.42	0.30
10-mer (3,8)	–0.67	0.23
10-mer (2,9)	–0.87	0.24
10-mer (1,10)	–1.14	0.04

[a)] (X,Y) indicates that the negative point charges are placed next to the Xth monomer and the Yth monomer at a distance of 7.5 Å unless otherwise noted; [b)]the negative point charges are placed at a distance of 5 Å.

With the ability to visualize each of the charged species established, **Table 1** examines the energetic stability of the different P3HT polaron and bipolaron species both with and without the presence of counterions. We calculate the binding energy of the bipolarons using the methodology described in the Experimental Section below. The way we define the bipolaron binding energy is that a positive binding energy means that forming a bipolaron takes less energy than forming two separate single polarons, so that bipolarons would form spontaneously whenever the chain is doubly-oxidized. A negative binding energy indicates that it is energetically more favorable to oxidize two different neutral segments of the polymer, creating two separate polarons, than to oxidize the same segment of the polymer twice and create a bound bipolaron.

In the absence of counterions, Table 1 shows that the binding energies of both singlet and triplet bipolarons on a 10-mer of P3HT are negative, which means that neither type of bipolaron is energetically bound. This is almost certainly a result of the fact that the system is not electrically neutral, and that positively-charged polarons will strongly repel each other no matter what their spin relationship. In real systems, however, whenever a conjugated polymer segment is oxidized, there always will be a counterion nearby. In chemical doping, the counterions are typically the anionic form of the dopant molecules used to oxidize the polymer. In electrochemical doping, the counterions are the anions of the electrolyte solution that are driven into the polymer film after the electrode removes charge from the material. The fact that chemical and electrochemical doping incorporate counterions into conjugated polymer films in different ways suggests that the counterions in films doped by these two methods are likely to reside in different locations relative to the positively-charged holes on the polymer backbone.

Scheme 2. Cartoon showing the various locations of the negative point charges used to represent the counterions for the 10-mer P3HT used in the TD-DFT calculations.

Thus, to understand how the counterion positions might affect the energetic stability of singlet and triplet bipolarons, we performed a series of calculations using six different positions of negative point charges to represent the counterions along our charged P3HT 10-mers. We placed the point charges in the plane of the thiophene rings to be consistent with experiments and simulations that have shown that dopant counterions sit in the lamellar regions of P3HT crystallites and not among the polymer π-stacks.[42,44] We denote a set of counterion positions as (X,Y), where X and Y mark the relative monomer position of the negative point charges, which are placed 7.5 Å away from the backbone, as experimentally documented for the position of the anions in F_4TCNQ-doped P3HT films.[35,42–44] We placed the two counterions on opposite sides of the polymer backbone, as depicted by the colored circles in **Scheme 2**. For one set of calculations, (black circles in Scheme 2, denoted "(5.5, 5.5) d = 5 Å"), the point charges were placed only 5 Å away from the P3HT backbone to better represent the experimental counterion distance in anion-exchanged doped P3HT films.[46]

Table 1 shows that when the counterions are included in the calculations, the binding energy of a triplet bipolaron, i.e., a pair of strongly coupled single polarons, is always positive, regardless of the counterion positions. This suggests that Coulombic attraction from the counterions are able to "hold" two single polarons in relatively close proximity, allowing them to interact with a favorable energy. This result is different from the studies by Bendikov and co-workers,[40,41] who used different DFT functionals than we employ here and who did not find any bipolaron stabilization energy, even in the presence of counterions.

In contrast, Table 1 also shows that the binding energy for singlet bipolarons remains negative in the presence of counterions, except for the case (5.5,5.5) d = 5 Å, where the counterions are both centered along the P3HT 10-mer and are as close as possible to the polymer backbone. This shows that not only are counterions needed for singlet bipolarons to form, but also that singlet bipolaron formation requires the two anions to be arranged in a highly specific geometry. Charges near the ends of the chain tend to pull the singlet bipolaron apart; only the Coulomb attraction from closely-spaced counterions can hold a singlet bipolaron together.

Experimentally, bipolarons are not observed to form until the doping level approaches one charge for every few P3HT repeat units. Thus, to test the limit of higher doping levels, we repeated the calculations for shorter P3HT oligomers with only 5 or 6 repeat units, roughly doubling the doping density of the P3HT 10-mer. Interestingly, the singlet bipolaron remains unbound even at these much higher effective polaron concentrations, explaining why singlet bipolarons are rarely observed in F_4TCNQ-doped P3HT films where the anions sit in the lamellar regions of crystalline domains at a distance of ≈7.5 Å away from the polymer backbone.[35,42–44] Even though singlet bipolarons remain unbound, they do become more stable than triplet bipolarons at higher doping levels. The reason for this can be seen in Scheme 1: for the same effective charge distribution, a singlet bipolaron distorts the P3HT backbone only once, but a triplet bipolaron distorts the backbone in two different locations. Thus, our calculations suggest that as the concentration of polarons increases, strongly coupled single polarons (triplet bipolarons) will form first, but then as the concentration of polarons continues to increase, stable singlet bipolarons will form.

We turn next to exploring the spectral signatures of polarons and singlet and triplet bipolarons on P3HT chains with different counterion positions. As described in the Experimental Section, we do this via TD-DFT calculations using the range-separated hybrid ωPBE functional to obtain realistic excited-state energy positions and transition dipoles; the results are shown in **Figure 3**. The solid and dashed black curves in both panels show the results for neutral P3HT and single P3HT polarons, respectively. Although the calculated P1, P2, and BG transitions are all bluer than seen experimentally, a known issue with DFT calculations on systems with extended π-conjugation, the calculated spectra do strongly resemble the experimental spectrum (shown below in Figure 5a).

Figure 3a shows the calculated spectra of a singlet bipolaron on a P3HT 10-mer with different counterion positions; in accord with Scheme 2, purple curves correspond to counterion positions near the center of the chain (the most energetically stable configurations; see Table 1) while red curves correspond to placing the counterions close to the chain ends (the least energetically stable configurations). As the singlet bipolaron is increasingly stabilized by moving the point charges nearer the chain center, its absorption spectrum shifts to the blue. For the one counterion configuration where the singlet bipolaron is energetically more stable than separate single polarons ((5.5,5.5) d = 5 Å), the calculated BP1 transition occurs at higher energies than the P1 band of the single polaron. Thus, our calculations are in agreement with the traditional picture in Scheme 1e, which predicts that stable singlet bipolarons absorb to the blue of single polarons.

In contrast, Figure 3b shows that the calculated spectra of triplet bipolarons, our proxy for strongly-coupled single polarons

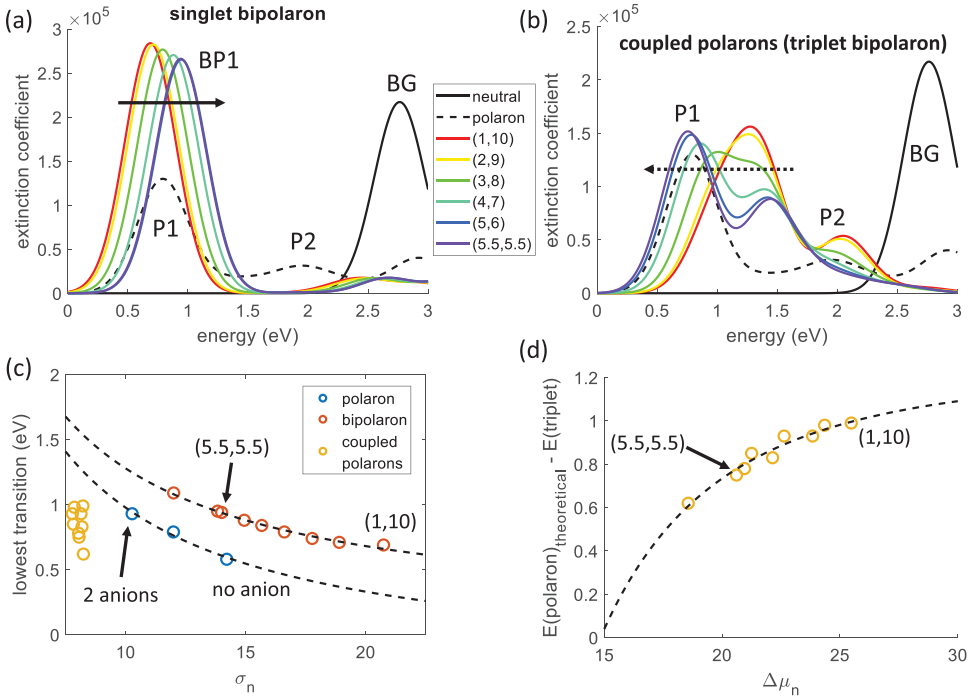

Figure 3. Absorption spectra, calculated using TD-DFT with the ωPBE functional and with PCM ($\varepsilon = 3$), for P3HT a) singlet bipolarons and b) coupled polarons (triplet bipolarons) for the different locations of the point-charge counterions shown in Scheme 2. (*X*, *Y*) indicates that the anions are placed along the *X*th and *Y*th monomers at a distance of 7.5 Å from the backbone. Red curves for (1,10) show the spectra with the anions near the ends of the chain. The counterion positions move toward the chain center in spectral order, with the purple curves for (5.5.,5.5) showing the absorption spectra with the anions positioned at the center of the chain. The absorption spectra of neutral P3HT (black solid curve) and a single P3HT polaron (black dashed curve) are also included. c) The energy of the lowest spectral transition, i.e., the position of the first peak in the absorption spectrum, as a function of the charge delocalization width (σ_n, calculated from fits like those in Figure 2) for polarons (blue circles), singlet bipolarons (red circles), and coupled polarons (triplet bipolarons; yellow circles). For the coupled polarons, σ_n is the average of σ_{n_1} and σ_{n_2}. d) The energy of the lowest transition for coupled polarons (triplet bipolarons) as a function of the distance between the two coupled polarons, $\Delta\mu_n = |\mu_{n1} - \mu_{n2}|$ (see the Supporting Information for more details). The dashed curve shows a fit to an inverse-cubed dependence, as expected for *J*-coupling between the two polarons' transition dipoles.

without a definite spin relationship, have the opposite behavior. The P1 peak starts out very blueshifted for coupled polarons with (1,10) or (2,9) counterion locations (red and orange in Figure 3b). For these two configurations, the counterions pull the pair of polarons to the opposite ends of the chain. Confining the polarons at the chain ends makes them less delocalized, which causes a spectral blueshift relative to the P1 transition of a single polaron in the chain center. When the counterions are positioned within a monomer or two of each other, however, the calculations predict that the absorption spectrum of the triplet bipolaron shifts to the red of the P1 transition of the single polaron.

This result strongly suggests that the redshifting spectrum seen by Enengl et al. in Figure 1[28] is due to strongly-coupled single polarons. As the electrochemical bias is initially increased and more counterions are driven into the film, the polarons start to couple together, creating the redshifted spectrum. Only at higher biases, which as we show experimentally below are accompanied by increased disorder that allows the counterions to get closer together, can the polarons can spin-pair, producing singlet bipolarons that absorbing to the blue of the single polaron, as evident in the data in Figure 1b and consistent with the traditional picture. This result also suggests that the Holstein Hamiltonian model of Spano and co-workers,[29] which does not include spin, also predicts a redshift due to coupling between single polarons that are not spin-paired.

Why would strongly-coupled single polarons (triplet bipolarons) and singlet bipolarons have their spectra shift in opposite directions as they more strongly interact with their counterions? To answer this question, we examined both the locations and coherence length of our calculated polarons and bipolarons using the same type of bond length analysis shown in Figure 2. We fit the changes in bond lengths for each case to a Gaussian distribution, yielding a central position (μ_n) and a width or delocalization length (σ_n) in units of the number of C—C bonds. We then correlated the energies of the calculated spectral peaks in Figure 3 with the positions and coherence lengths of the corresponding (bi)polaronic species.

Figure 3c shows the energy of the lowest-energy spectral transition as a function of the delocalization length for single polarons (blue circles) and singlet bipolarons (red circles) on a P3HT 10-mer. For single polarons, as counterions are added, Coulomb attraction causes the polaron to become less delocalized, leading to a spectral blueshift; this is in accord with both experiments and the predictions of the Holstein Hamiltonian model.[35] For singlet bipolarons, as the anions move toward the middle of the chain, Coulomb attraction causes the delocalization length to decrease. Conversely, when the anions are located at the ends of the chain, Coulomb forces tend to pull the two bipolaron charges apart, causing the singlet bipolaron to become more delocalized. Thus, it makes sense that for

both polarons and singlet bipolarons, the energy of the lowest spectral transition is inversely related to the delocalization length, which is controlled by the number and position of the counterions.

For two coupled polarons on a P3HT 10-mer (i.e., triplet bipolarons), the yellow circles in Figure 3c show that there is no correlation between the energy of the lowest transition and the polaron delocalization length (plotted as the average width of the two Gaussians used to fit the change in bond lengths). Instead, Figure 3d shows that the energy of the lowest transition is related to the distance between the two coupled single polarons: as the distance between the two polarons decreases, the absorption spectrum redshifts. Since the transition dipole moment of the lowest-energy polaronic transition lies along the chain axis,[47] two nearby polarons have aligned transition dipoles that can *J*-couple.[48–50] For *J*- (and *H*-) aggregation, coupling causes an energy splitting that is inversely proportional to the cube of the distance between the two chromophores. For *J*-aggregates, the lower state carries the oscillator strength, so as the distance between the chromophores decreases, the absorption spectrum redshifts. As the counterions are moved from the ends of the chain to the middle of the chain, Coulomb attraction causes the distance between the two coupled polarons to decrease, making the coupling stronger and causing the absorption spectrum to redshift. The black dashed curve in Figure 3d shows a fit to an inverse-cubic dependence, verifying that the spectral redshift is indeed due to coupling between the transition dipoles of two essentially independent polaronic chromophores.

All of the above calculations show that, as the doping density increases, single polarons can begin to have their transition dipoles *J*-couple. This leads to a redshifted absorption spectrum like that seen by Enengl et al. in Figure 1[28] and by Spano and co-workers' Holstein Hamiltonian-based bipolaron model.[29] Only when the doping density gets high enough and the counterions are appropriately positioned can two polarons spin-pair, leading to a blueshifted absorption spectrum and a decreased EPR signal. It is important to note, however, that not every experiment shows a significantly redshifted or blueshifted polaronic absorption at higher doping levels, which suggests that the difference between different experiments is due to the positions of the counterions. The positions of the counterions, in turn, depend both on the counterion identity and whether the counterions were introduced by chemical or electrochemical doping (and on the exact nature of both of those processes). We thus turn to explore the conditions under which coupled single polarons and singlet bipolarons can form experimentally in the next section.

2.2. Creation of Coupled Polarons and Bipolarons via Electrochemical and Chemical Doping Methods in P3HT

The electrochemical doping experiments by Enengl et al. reproduced in Figure 1a show clear evidence for a redshifted polaronic absorption band as the doping level is increased to ≈800 mV potential relative to Ag/AgCl.[28] In Figure 1b, however, at slightly higher oxidation potentials, there also appears to be a new blueshifted absorption in the region near 1.0 eV,

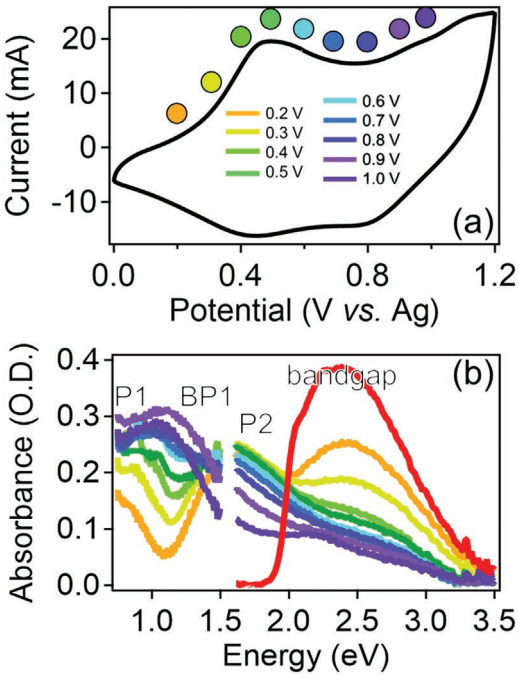

Figure 4. a) Cyclic voltammetry of a P3HT thin film on an indium tin oxide (ITO) substrate over the potential range of 0 V to +1.2 V versus Ag/Ag^+ in a 0.1 M lithium perchlorate ($LiClO_4$) in propylene carbonate solution. b) In situ absorption spectra of the electrochemically-doped film whose CV is shown in panel (a) at different potentials versus Ag/Ag^+. The color of the absorption spectrum curves in panel (b) corresponds to the colored circles on the CV curves in panel (a). The data are similar to those from Enengl et al. in Figure 1,[28] but the decreased P2 absorption and new BP1 absorption to the blue of P1 (and corresponding isosbestic point at 1.4 eV) at high oxidation potentials are more clearly shown. Reliable absorption data could not be taken near ≈1.6 eV due to a detector change in the instrument.

accompanied by an isosbestic point near 1.4 eV that indicates the production of a new chemical species. Thus, the change in EPR signal observed by Enengl et al.[28] might be associated with the blue ≈1.0 eV absorption shoulder rather than the ≈0.3 eV redshifted polaronic absorption since both exist at similar oxidation potentials. The fact that the ≈0.3 and ≈1.0 eV absorption bands do not appear simultaneously, however, unambiguously shows that these two features are associated with different electronic species.

To better understand the outcomes obtained by Enengl et al.,[28] we performed chemical and electrochemical doping experiments on P3HT films to produce polarons and bipolarons, as shown below in **Figures 4** and **5**. In the electrochemical doping experiments (Figure 4), electrons are removed from the polymer film at the electrode, and a counterion is brought in from the electrolyte for charge-balance. In contrast, chemical doping of conjugated polymers involves a redox process involving the dopant molecule that then becomes the charge-balancing counterion. To compare these two modes of doping, we also chemically doped P3HT with a strong oxidant, iron (III) chloride ($FeCl_3$), which is able to produce both polarons and bipolarons and which creates absorption features at both ≈0.3 and ≈1.0 eV (Figure 5). Additionally, in the Supporting Information, we explore the role of how swelling of the

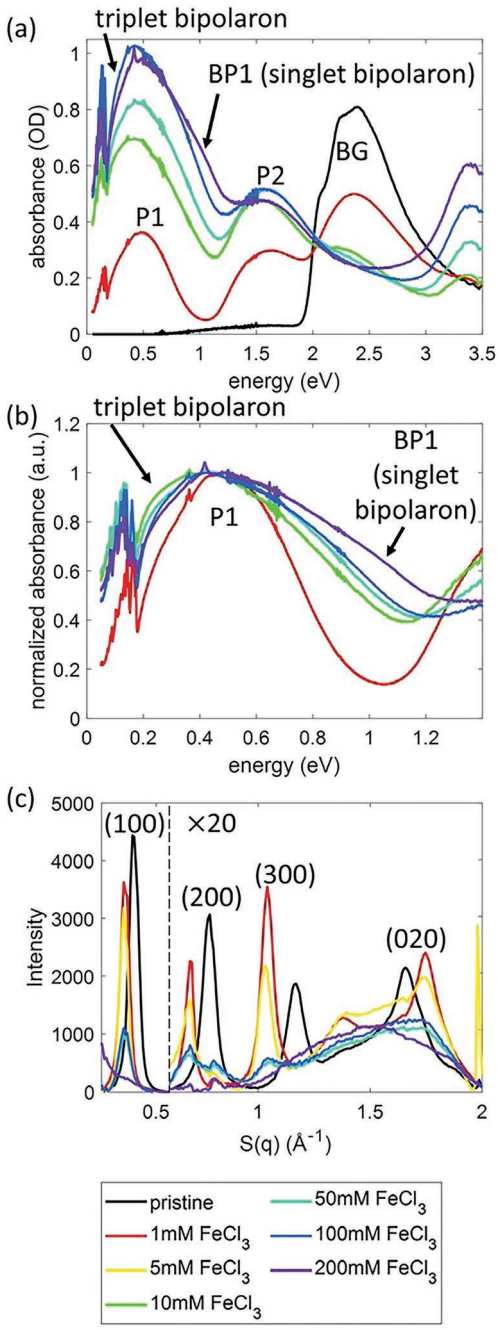

Figure 5. a) Absorption spectra, b) normalized absorption spectra, and c) radially-integrated 2-D grazing-incidence wide-angle X-ray diffraction pattern of P3HT films sequentially doped with different concentrations of $FeCl_3$. For panel (b), the absorption spectra are normalized by the maximum absorbance of the P1 peak near 0.5 eV. The data in panels a and b clearly show that as the doping concentration increases, the absorption of coupled polarons to the red of P1, near 0.3 eV appears first, and then this absorption and both P1 and P2 decrease as the new BP1 band appears near 1.0 eV, with isosbestic points near 0.7 and 1.4 eV. In panel (c), the vertical axis scale changes at 0.6 Å^{-1}, indicated by the vertical dashed line. To the right of the scale break, the *y*-axis is expanded by a factor of 20 to better show the (h00) overtones and the (020) peak. The data show clearly that bipolaron formation is accompanied by a loss of crystalline structure.

polymer controls counterion localization and thus determines whether bipolarons can be formed (Figure S10, Supporting Information). Finally, we show that only the ≈1.0 eV absorbing species is associated with a structural change (loss of crystallinity) in the doped P3HT film, further verifying that the two absorption bands are independent electronic species. By using different doping mechanisms and solvents that swell the polymer films to different extents, we are able to correlate spectroscopic features with structural changes, and thus produce a coherent picture of doping based on the positions of the counterions in the doped polymer films.

For our electrochemical doping experiments, we cycled a P3HT film in the potential window of 0 V to + 1.2 V versus Ag/Ag^+ with a 0.1 M $LiClO_4$ electrolyte in propylene carbonate to create polarons and bipolarons. Figure 4a shows the cyclic voltammetry (CV), which displays a clear oxidation peak starting at 0.2 V versus Ag/Ag^+, and a second smaller oxidation peak between 0.8 and 1.0 V versus Ag/Ag^+. The colored circles above the CV curve represent points at which absorption spectra were taken in situ while holding the potential fixed. These spectra are shown with matching colors in Figure 4b. When there is no applied potential, the red curve in Figure 4b shows the neutral bandgap (BG) peak of P3HT, centered at 2.5 eV. As the potential is increased to roughly 400 mV versus Ag/Ag^+, the bandgap peak decreases and polaronic absorption peaks appear, one centered at ≈1.5 eV (P2) and the other off the red edge of our spectral window (P1). As the potential is further increased, the P2 absorption band then starts to decrease and an obvious new absorption peak appears near 1.1 eV, with an isosbestic point between them near 1.4 eV. This clearly indicates that single polarons are being converted to a new chemical species with an absorption spectrum that lies well to the blue of the P1 absorption band, and that the new chemical species forms at higher oxidation potentials.

All these observations, which mirror those seen in this same spectral region by Enengl et al. (cf. Figure 1b),[28] are consistent with the idea that singlet bipolarons are being formed by doubly-oxidizing the P3HT backbone, and that these bipolarons have a BP1 peak that is bluer than the single polaron P1 band. This result is consistent with both the traditional picture in Scheme 1 and our TD-DFT calculations discussed above. The energy to create singlet bipolarons is ≈0.3 eV greater than the energy to form single polarons, and we will discuss the origins of that energy difference below.

As mentioned above, in electrochemical doping, the electrode removes electrons from the P3HT backbone, and a counterion from solution is subsequently recruited into the solvent-swollen polymer film to balance the charge. This gives the counterions a lot of flexibility in finding their final locations, creating the possibility that counterions can reside in the most energetically favorable location to stabilize the singlet bipolaron. In contrast, in chemical doping, the counterions are produced by the redox process involving the dopant. Thus, the counterions tend to be trapped in the film wherever the dopant originally resided, as diffusion of traditional large dopant molecules like F_4TCNQ is slow. This may make it less likely for two counterions to reside very close together, which based on our TD-DFT calculations, is required to stabilize a singlet bipolaron. These ideas thus provide a possible explanation for why chemical doping may be less likely to produce singlet bipolarons than electrochemical doping.

To test this hypothesis experimentally, we chemically doped P3HT films with different concentrations of $FeCl_3$ using sequential processing (SqP);[35,51,52] the results are shown in Figure 5. Several groups have argued that $FeCl_3$ has a high enough oxidation potential to ionize P3HT chains twice, allowing for the potential creation of bipolarons.[53] Additionally, Yamamoto et al.[54] showed that both vapor-phase and solution-phase doping of P3HT with $FeCl_3$ initially results in polarons and that longer exposure time leads to the formation of bipolarons. We focus on $FeCl_3$ both because of its high oxidizing potential, which allows energetically for the possibility of making bipolarons, and because it is quite small, allowing its counterions to have more mobility in doped P3HT films and thus providing the possibility of optimizing the counterion location to stabilize singlet bipolarons.

Figure 5a shows that as the concentration of $FeCl_3$ increases, P3HT films become more doped, as evidenced by a decrease in the bandgap absorption near 2.5 eV and large increases in the polaronic P1 and P2 absorption bands near 0.5 and 1.6 eV, respectively. Figure 5b shows the red portion of the absorption spectra with the data normalized at 0.5 eV to more easily compare the spectral shapes at different doping concentrations. The data show that at low $FeCl_3$ doping concentrations (1 mM), only single polarons are formed. As the $FeCl_3$ concentration is increased to 10–50 mM and the films become more doped, we see a redshift of the P1 peak, exactly along the lines of that observed by Enengl et al. in Figure 1[28] and our TD-DFT calculations from the previous section, which we believe reflects the formation of strongly coupled single polarons (or triplet bipolarons). We note that when P3HT is doped with a highly-oxidizing functionalized dodecaborane-based dopant, a similar spectral redshift is also observed,[36,55] but no such redshifts are seen with F_4TCNQ, which likely does not have enough oxidizing power to create polarons that are close enough together to *J*-couple.

As the $FeCl_3$ doping concentration is further increased to between 100 and 200 mM, the red shoulder indicative of the formation of coupled polarons starts to disappear, and a new absorption band near 1.1 eV appears, accompanied by isosbestic points at 0.7 and 1.4 eV. All of these features are consistent with the idea that there are now enough counterions in the correct positions to allow for the formation of singlet bipolarons. Some of the previously strongly-coupled single polarons are now spin-paired, so their redshifted P1 absorption and accompanying P2 absorption disappear and are replaced by the blueshifted BP1 absorption at 1.1 eV, exactly in accord with the traditional picture in Scheme 1 and our TD-DFT calculations. Interestingly, this same conversion of coupled single polarons to singlet bipolarons is not seen with the highly oxidizing dodecaborane-based dopants studied previously, even though they have a similar oxidation potential to $FeCl_3$.[36,55] This is because the dodecaborane counterions are too large to allow them to get close enough together to provide the necessary Coulomb stabilization for the singlet bipolaron.

Given that it is now clear that singlet bipolarons can be created both electrochemically and chemically, it is worth considering the following question: why there is only partial conversion of single polarons into singlet bipolarons in the $FeCl_3$-chemically-doped P3HT films and in the electrochemically-doped films studied in Figure 1, but there is almost full conversion in the electrochemically-doped films presented in Figure 4? Since the presence of different polaronic species depends sensitively on the counterion positions, this difference likely reflects a change in structure of polymer films doped by different methods. We thus have looked for such structure changes using grazing-incidence wide-angle X-ray scattering (GIWAXS).

Figure 5c shows GIWAXS diffractograms of the $FeCl_3$-doped films whose absorption spectra are shown in Figure 5a,b. Prior to any dopant being introduced to P3HT (black curve), we see the (100) principle lamellar peak located at 0.38 $Å^{-1}$, along with two overtones, as well as a clear (020) π-stacking peak near 1.7 $Å^{-1}$. At low $FeCl_3$ doping concentrations (< 10 mM), where the absorption spectrum suggests only isolated single polarons are formed, the lamellar peak shifts to lower q, while the π-stacking peak shifts to higher q. These structural signatures, which correspond to an expansion of the crystal lattice in the lamellar direction and a change in tilt of the unit cell,[56] have been seen in numerous doped conjugated polymers with a plethora of dopants.[35,51,52,57] As the doping concentration increases to the point where singlet bipolarons start to form (≥ 50 mM), the lamellar overtones decrease in intensity, indicating that the polymer crystallites are beginning to disorder. This is consistent with the observations of Banerji and co-workers, who have argued that bipolarons form in disordered regions of the polymer films first.[58] At the highest $FeCl_3$ dopant concentration, where the absorption suggests that singlet bipolarons are becoming the dominant species, even the π-stacking peak, which is a very robust feature of almost all conjugated polymers, has disappeared, indicating that the films have become almost entirely amorphous.

The fact that the red-shifted P1 band does not appear simultaneously with the blue-shifted band and that the blue-shifted band is associated with a structural change in the doped P3HT film shows clearly that red- and blue-absorption features belong to two entirely different electronic species. It is certainly possible that these two species could be something like intra- and inter-chain singlet bipolarons, but given the DFT calculations in the previous section, we believe that the simplest assignment is that the red-absorbing species is strongly-coupled single polarons while the blue-absorbing species corresponds to singlet bipolarons.

This assignment is supported by the fact that the crystallinity of P3HT begins to lower at precisely the same dopant levels as singlet bipolarons start to form, which is a clear experimental signature that counterion location is important in the formation of singlet bipolarons. When P3HT is strongly crystalline, dopant counterions are generally confined to the lamellar region, far from the backbone and in lower density, where they are unable to provide the stabilization necessary to create singlet bipolarons. At higher dopant concentrations, more counterions are needed, and eventually, the number of counterions exceeds the capacity of the crystalline polymer network. This necessitates disordering the polymer. Once that disordering occurs, however, the counterions can then more flexibly arrange around the P3HT backbone to stabilize singlet bipolaron formation. Thus, bipolaron formation and a loss of crystallinity are coupled, because the latter is required to allow counterions to provide the necessary Coulomb stabilization.

The disordering of the crystalline polymer network comes at an energetic cost, and is likely part of the ≈0.3 eV energy difference between the polaron and the bipolaron observed in in the CV curves in Figure 4.

With these ideas in hand, it is now possible to understand why singlet bipolaron formation does not occur equally in all systems. The key difference involves how the different doping methodologies swell the polymer films. We describe the way in which we quantify swelling, by the mass gain when the polymer is exposed to the vapor of the different solvents, in the Supporting Information. The electrochemical doping data in Figure 4 was collected using propylene carbonate (PC) as a solvent, and PC is an effective swelling solvent for P3HT, gaining 22% mass after being allowed to swell in the presence of PC vapor (Figure S8, Supporting Information). As a result this swelling, two things happen. First, because the films are swollen by the electrolyte solution, the necessary structural reorganization and loss of crystallinity needed for bipolaron formation can take place with less energetic penalty. Second, the swollen polymer environment allows for facile counterion diffusion so the counterions can easily move to locations that can optimally stabilize bipolarons. By contrast, the data of Enengl et al. in Figure 1 was taken using an acetonitrile-based electrolyte, and acetonitrile is a very poor swelling solvent for P3HT, gaining no measurable weight within error after exposure to acetonitrile vapor. For our chemical doping experiments with $FeCl_3$, *n*-butylacetate (*n*-BA) was used to introduce the dopant, a solvent which swells P3HT significantly, producing a 60% mass increase after being allowed to swell in *n*-BA vapor. Based on swelling alone, one might expect doping in *n*-BA to produce the most singlet bipolarons. However, the fact that the oxidizing equivalent and counterion are delivered together does not allow time for the counterions to find the optimal location to stabilize singlet bipolarons. This means that chemical doping with a swelling solvent and electrochemical doping with a very poor swelling solvent produce similar results (Figures 1 and 5). Only electrochemical doping in a reasonable swelling solvent produces significant amounts of singlet bipolarons (Figure 4).

Finally, we note that in addition to the fact that dopants like F_4TCNQ are likely not oxidizing enough to produce singlet bipolarons, the fact that the incorporation of their counterions does not significantly reduce the crystallinity of P3HT[57,59] provides an additional energetic barrier to the creation of singlet bipolarons. Overall, a broad range of data paints a coherent picture of the conditions needed to stabilize singlet bipolaron formation. The conclusions from our TD-DFT calculations are that the counterion positions control the nature of the oxidized species at high doping concentrations in P3HT. This is born out in real experimental systems where counterion location is either more rigidly controlled through crystallinity, or allowed to be more flexible in amorphized materials.

3. Conclusion

Using both calculations and experiments, we have explored how the energies and the absorption spectra of single polarons, coupled single polaron (triplet bipolarons) and singlet bipolarons on doped conjugated polymers are affected by counterion positions. Without counterions, neither singlet bipolarons nor coupled single polarons are energetically bound, but with counterions in the right locations, both coupled single polarons and singlet bipolarons can form. When the counterions are placed at the middle of a chain, singlet bipolarons can stably form, with an absorption peak that is blue of the polaron P1 band; this blue shift results because the singlet bipolaron is less delocalized because of coulomb attraction to the high counterion density at the chain center. For other counterion positions, strongly-coupled single polarons are the most stable species, with an absorption spectrum that lies to the red of the P1 transition because of *J*-coupling between the transition dipoles of the individual polarons.

Taken together, our results allow us to propose the following model for the order of formation for single polarons, coupled single polarons, and singlet bipolarons upon increased doping of conjugated polymers:

1) Initially, at low doping concentrations for either chemical or electrochemical doping, only single polarons are formed. In this regime, there are plenty of neutral polymer segments of polymer that are kinetically convenient to be oxidized. The polarons that are formed have the traditional P1 and P2 absorption bands, and the BG transition decreases in intensity. At this stage, no coupled polarons or singlet bipolarons can form because of the low density of polarons and counterions.
2) As more segments of the polymers are oxidized and additional counterions are incorporated into the polymer film, coupled polarons and singlet bipolarons begin to form depending on the local positions of the counterions. Since the counterion position for creating singlet bipolarons is more restrictive, the red-shifted spectral signatures of strongly-coupled polarons generally appear before the blue-shifted signatures associated with singlet bipolarons. The exact spectral changes, however, depend on the oxidizing potential of the dopant or applied electrochemical bias, the size and mobility of the counterions in the doped polymer film, the crystallinity of the polymer film, and the extent of solvent swelling.
3) Finally, as the doping concentration continues to increase, the polymer crystallites are unable to accommodate all of the counterions in an ordered manner, so the crystalline structure of the doped polymer film is disrupted. The energetic cost to disorder the polymer film is part of the increased redox energy required to produce highly-doped polymer films. Once disordering occurs, counterions can move so that both single polarons and strongly-coupled polarons can spin-pair into singlet bipolarons. The spectral signatures of this are a decrease in the P1 and P2 single-polaron absorption band intensities and a growth of the BP1 absorption band at energies in between. A signature of this transformation are the isosbestic points between the P1/BP1 and P2/BP1 bands, which in doped P3HT occur near 0.7 and 1.4 eV, respectively.

Overall, all of our work suggests that the traditional band picture for polarons and bipolarons in doped conjugated polymers is correct;[27,62] the "new" spectral signature that appears to the red of P1 results from the interaction between strongly-coupled, but not spin-paired polarons. Understanding the production sequence of the different polaronic species on doped conjugated polymers

is important for their applications. In general, the formation of polarons, rather than bipolarons, is desirable, as bipolarons generally have poor mobility and their presence is associated with a decrease in electrical conductivity. Our results not only have identified spectral signatures of coupled polarons and singlet bipolarons, but also present design rules for preventing or enhancing their formation: the use of large, bulky counterions in rigidly crystalline films favors polaron formation, whereas small mobile counterions in poorly crystalline films (such as those swollen with solvent during electrochemical doping) favor bipolaron formation. Thus, the proper choice of doping method and counterion allows the creation of highly doped films with minimal bipolaron formation and thus maximum electrical conductivity, leading to improved optoelectronic devices.

4. Experimental Section

Calculations: DFT (density functional theory) and TD-DFT (time-dependent density functional theory) calculations were done using the Gaussian 09 program. The calculations focused on P3HT oligomers with either 5, 6, or 10 monomers. These oligomer lengths were chosen because Stanfield et al.[43] recently demonstrated that polarons in doped P3HT have a spatial extent of ≈5 to 7 repeat units, depending on the P3HT crystallinity, so that these lengths were sufficient to capture polaron and singlet bipolaron behavior without significant computational expense. For the triplet bipolaron, the use of a longer chain might led to additional delocalization of the two coupled polarons. However, this would further redshift the calculated absorption spectrum of the coupled polarons, reinforcing the conclusions reached in the main text.

To further reduce the computational cost, the P3HT hexyl side chains in the calculations were replaced by methyl groups and the oligomer chains were also methyl terminated. The calculations were performed on neutral oligomers as well as oligomers with either one or two electrons removed; when electrons were removed, sometimes negative point charges were also added at various positions, as described in Scheme 2, to ensure that the system was electrically neutral. For the case of the doubly-charged oligomers, calculations were performed with both multiplicity = 1 (singlet bipolaron) and multiplicity = 3 (triplet bipolaron, used as a proxy for strongly-coupled, but unpaired single polarons). For the singlet bipolaron, only the closed-shell state was considered, as there was no easy way to investigate the possibility of singlet bipolarons with open-shell character. The stability of the wavefunctions was tested for the singlet bipolaron state for the P3HT 5-mer, 6-mer, and 10-mer both with and without counterions. All were found to have RHF → UHF instability, which was not surprising because the energy of the triplet state was close to and sometimes lower than the energy of the closed-shell singlet state. It was believed, however, that open-shell singlet bipolarons would behave essentially identically to triplet bipolarons and thus serve as another proxy for strongly-coupled single polarons.

All systems studied were geometry-optimized using the 6-31G** basis set and the PBE0 functional with a polarizable continuum model (PCM) with ε = 3, chosen to match the experimentally-measured dielectric constant of P3HT.[60] TD-DFT calculations were then performed on the optimized structures using the 6-31G** basis set and the long-range corrected *ω*PBE functional. The geometry was not optimized using the long-range corrected *ω*PBE functional both because this functional was computationally more expensive and because the use of this functional caused the polaron to localize on one end of the chain rather in the middle, which was not believed to be realistic. When geometry optimizing the charged oligomers in the presence of negative point charges, the positions of the methyl groups at the ends were fixed and the S—C—C—S inter-ring dihedral angles were fixed at 180 degrees. This prevented the positively charged oligomers from drifting toward the negative point charges.

The binding energies of bipolarons with and without counterions were calculated as follows:

$$\text{Binding Energy} = 2 \times E_{\text{f,polaron}} - E_{\text{f,bipolaron}} \tag{1}$$

where $E_{\text{f,polarons}}$ and $E_{\text{f,bipolarons}}$, the energy of formation for a polaron and a bipolaron, are:

$$E_{\text{f,polaron}} = E_{\text{polaron w/one anion}} - E_{\text{neutral w/one anion}} \tag{2}$$

$$E_{\text{f,bipolaron}} = E_{\text{bipolaron w/two anions}} - E_{\text{neutral w/two anions}} \tag{3}$$

and $E_{X\ \text{w/}N\ \text{anion(s)}}$ is the energy of the neutral oligomer, polaron, or bipolaron with N anion(s). The bipolaron binding energy is defined such that a positive binding energy means that forming a bipolaron takes less energy than forming two separate single polarons and a negative binding energy indicates that it is energetically more favorable to oxidize two different neutral segments of the polymer, creating two separate polarons, than to oxidize the same segment of the polymer twice and create a bound bipolaron.

Figure S1 (Supporting Information) shows the changes in the Mulliken charges between the neutral and the charged species for each monomer. Both the changes in the partial charges and the changes in bond lengths give qualitatively similar description for the position and the delocalization of the polaron/bipolaron.

Figures S3–S5 (Supporting Information) show the fits of the change in bond lengths curves to sums of Gaussian distributions to get the central position (μ_n) and the width of delocalization length (σ_n) in units of C—C bond lengths. For single polarons and singlet bipolarons, the change in bond lengths were fitted with a single Gaussian function.

$$\Delta(\text{bond length})(\mu_n, \sigma_n) = A \exp\left[-\frac{1}{2}\left(\frac{b-\mu_n}{\sigma_n}\right)^2\right] \tag{4}$$

For triplet bipolarons/pairs of coupled single polarons, the change in bond lengths curves were fitted to the sum of two Gaussian functions.

$$\Delta(\text{bond length})(\mu_{n_1}, \mu_{n_2}, \sigma_{n_1}, \sigma_{n_2}) = A_1 \exp\left[-\frac{1}{2}\left(\frac{b-\mu_{n_1}}{\sigma_{n_1}}\right)^2\right] + A_2 \exp\left[-\frac{1}{2}\left(\frac{b-\mu_{n_2}}{\sigma_{n_2}}\right)^2\right] \tag{5}$$

Experiments: Doped P3HT films were prepared by sequential processing (SqP), where undoped P3HT films were first made by spin coating, and then the dopant (either F_4TCNQ or $FeCl_3$) was introduced in a second spin coating step from a semi-orthogonal solvent that swells, but does not dissolve the film. Electronic-grade regioregular P3HT (4002-EE; 91–94%, Mw = 46–57 kg mol^{-1}, PDI = 2.3) was purchased from Rieke Metals, $FeCl_3$ was purchased from EM Science, and all solvents were purchased from Sigma–Aldrich. All materials and solvents were used as received without any further purification, unless otherwise stated

For $FeCl_3$-doped P3HT films, 20 mg mL^{-1} of P3HT was dissolved in *o*-dichlorobenzene (ODCB) at room temperature and stirred overnight. The dopant solution was prepared immediately before use by dissolving appropriate amount of $FeCl_3$ in *n*-BA. Undoped P3HT films were made by spin-coating 10 µL of the P3HT solution on glass at 1000 RPM for one minute. The films were then doped by letting 50 µL of the $FeCl_3$ solution soak the films for 120 s followed by spinning at 4000 RPM for 10 s to remove excess $FeCl_3$ solution.

Cyclic voltammetry (CV) was carried out on a VMP potentiostat/galvanostat (Bio-Logic). The working electrode is a P3HT film on ITO, the reference is silver wire, and the counter electrode is platinum sputtered onto an ITO substrate. The electrolyte was composed of 0.1 M

lithium perchlorate ($LiClO_4$) in propylene carbonate (PC). To collect spectroelectrochemistry in situ, the potential of interest was applied during the entire data collection period.

UV–vis–NIR absorption spectra were acquired from 300–2500 nm using a Shimadzu UV3101PC Scanning Spectrophotometer. FTIR data was acquired from 220–7000 cm^{-1} for matched samples deposited on KBr plates using a Jasco FT/IR-420 spectrometer.

To understand the structural changes of heavily doped P3HT, matched $FeCl_3$-doped films were made on 1.5 cm^2 Si substrates with a <100> orientation. Measurements were performed at the Advanced Photon Source on beamline 8ID-E with X-ray energy of 10.92 KeV, at an incident angle of 0.14 with the detector distance at 217 mm. Gap-filling and integrations of the 2D diffractograms was performed on the MATLAB toolbox GIXGUI.[61]

Supporting Information

Supporting Information is available from the Wiley Online Library or from the author.

Acknowledgements

E.C.W. and C.Z.S. contributed equally to this work. This work was supported by the National Science Foundation under grant numbers CHE-2003755 and DMR-2105896. This research used resources of the Advanced Photon Source, a U.S. Department of Energy (DOE) Office of Science User Facility, operated for the DOE Office of Science by Argonne National Laboratory under Contract No. DE-AC02-06CH11357. The authors would like to thank Frank Spano at Temple University for stimulating discussions.

Conflict of Interest

The authors declare no conflict of interest.

Data Availability Statement

The data that support the findings of this study are available from the corresponding author upon reasonable request.

Keywords

bipolarons, chemical doping, counterions, electrochemical doping, polarons, semiconducting polymers

Received: November 23, 2022
Revised: January 20, 2023
Published online:

[1] L. Dou, J. You, Z. Hong, Z. Xu, G. Li, R. A. Street, Y. Yang, *Adv. Mater.* **2013**, *25*, 6642.
[2] M. Kuik, G.-J. A. H. Wetzelaer, H. T. Nicolai, N. I. Craciun, D. M. De Leeuw, P. W. M. Blom, *Adv. Mater.* **2014**, *26*, 512.
[3] B. Russ, A. Glaudell, J. J. Urban, M. L. Chabinyc, R. A. Segalman, *Nat. Rev. Mater.* **2016**, *1*, 16050.
[4] J. S. Cowart, C. Liman, A. Garnica, Z. A. Page, E. Lim, R. R. Zope, T. Baruah, C. J. Hawker, M. L. Chabinyc, *Inorg. Chim. Acta* **2017**, *468*, 192.
[5] L. Hou, X. Zhang, G. F. Cotella, G. Carnicella, M. Herder, B. M. Schmidt, M. Pätzel, S. Hecht, F. Cacialli, P. Samorì, *Nat. Nanotechnol.* **2019**, *14*, 347.
[6] W. T. Choi, A. J. Bard, *J. Phys. Chem. C* **2020**, *124*, 3439.
[7] C. G. Bischak, L. Q. Flagg, K. Yan, T. Rehman, D. W. Davies, R. J. Quezada, J. W. Onorato, C. K. Luscombe, Y. Diao, C.-Z. Li, D. S. Ginger, *J. Am. Chem. Soc.* **2020**, *142*, 7434.
[8] J. E. Anthony, A. Facchetti, M. Heeney, S. R. Marder, X. Zhan, *Adv. Mater.* **2010**, *22*, 3876.
[9] J. L. Bredas, G. B. Street, *Acc. Chem. Res.* **1985**, *18*, 309.
[10] M. Nowak, S. D. D. V. Rughooputh, S. Hotta, A. J. Heeger, *Macromolecules* **1987**, *20*, 965.
[11] D. Beljonne, J. Cornil, H. Sirringhaus, P. J. Brown, M. Shkunov, R. H. Friend, J.-L. Brédas, *Adv. Funct. Mater.* **2001**, *11*, 229.
[12] C. Wang, D. T. Duong, K. Vandewal, J. Rivnay, A. Salleo, *Phys. Rev. B* **2015**, *91*, 085205.
[13] J. Fuzell, I. E. Jacobs, S. Ackling, T. F. Harrelson, D. M. Huang, D. Larsen, A. J. Moulé, *J. Phys. Chem. Lett.* **2016**, *7*, 4297.
[14] N. Colaneri, M. Nowak, D. Spiegel, S. Hotta, A. J. Heeger, *Phys. Rev. B* **1987**, *36*, 7964.
[15] E.-G. Kim, J.-L. Brédas, *J. Am. Chem. Soc.* **2008**, *130*, 16880.
[16] W. Shi, T. Zhao, J. Xi, D. Wang, Z. Shuai, *J. Am. Chem. Soc.* **2015**, *137*, 12929.
[17] P. Das, B. Zayat, Q. Wei, C. Z. Salamat, I.-B. Magdău, R. Elizalde-Segovia, D. Rawlings, D. Lee, G. Pace, A. Irshad, L. Ye, A. Schmitt, R. A. Segalman, T. F. Miller, S. H. Tolbert, B. S. Dunn, S. R. Narayan, B. C. Thompson, *Chem. Mater.* **2020**, *32*, 9176.
[18] L. Groenendaal, F. Jonas, D. Freitag, H. Pielartzik, J. R. Reynolds, *Adv. Mater.* **2000**, *12*, 481.
[19] N. Salem, M. Lavrisa, Y. Abu-Lebdeh, *Energy Technol.* **2016**, *4*, 331.
[20] E. M. Thomas, E. C. Davidson, R. Katsumata, R. A. Segalman, M. L. Chabinyc, *ACS Macro Lett.* **2018**, *7*, 1492.
[21] M. P. Gordon, S. A. Gregory, J. P. Wooding, S. Ye, G. M. Su, D. S. Seferos, M. D. Losego, J. J. Urban, S. K. Yee, A. K. Menon, *Appl. Phys. Lett.* **2021**, *118*, 233301.
[22] Y. Harima, R. Patil, H. Liu, Y. Ooyama, K. Takimiya, T. Otsubo, *J. Phys. Chem. B* **2006**, *110*, 1529.
[23] J. E. Cochran, M. J. N. Junk, A. M. Glaudell, P. L. Miller, J. S. Cowart, M. F. Toney, C. J. Hawker, B. F. Chmelka, M. L. Chabinyc, *Macromolecules* **2014**, *47*, 6836.
[24] V. Vijayakumar, P. Durand, H. Zeng, V. Untilova, L. Herrmann, P. Algayer, N. Leclerc, M. Brinkmann, *J. Mater. Chem. C* **2020**, *8*, 16470.
[25] L. Chen, W. Wang, S. Xiao, X. Tang, *Chin. Phys. B* **2022**, *31*, 028507.
[26] K. Al Kurdi, S. A. Gregory, M. P. Gordon, J. F. PonderJr, A. Atassi, J. M. Rinehart, A. L. Jones, J. J. Urban, J. R. Reynolds, S. Barlow, S. R. Marder, S. K. Yee, *ACS Appl. Mater. Interfaces* **2022**, *14*, 29039.
[27] M. G. Voss, J. R. Challa, D. T. Scholes, P. Y. Yee, E. C. Wu, X. Liu, S. J. Park, O. León Ruiz, S. Subramaniyan, M. Chen, S. A. Jenekhe, X. Wang, S. H. Tolbert, B. J. Schwartz, *Adv. Mater.* **2021**, *33*, 2000228.
[28] C. Enengl, S. Enengl, S. Pluczyk, M. Havlicek, M. Lapkowski, H. Neugebauer, E. Ehrenfreund, *ChemPhysChem* **2016**, *17*, 3836.
[29] M. B. Qarai, R. Ghosh, F. C. Spano, *J. Phys. Chem. C* **2021**, *125*, 24487.
[30] R. Ghosh, C. K. Luscombe, M. Hambsch, S. C. B. Mannsfeld, A. Salleo, F. C. Spano, *Chem. Mater.* **2019**, *31*, 7033.
[31] A. R. Chew, R. Ghosh, V. Pakhnyuk, J. Onorato, E. C. Davidson, R. A. Segalman, C. K. Luscombe, F. C. Spano, A. Salleo, *Adv. Funct. Mater.* **2018**, *28*, 1804142.
[32] R. Ghosh, C. M. Pochas, F. C. Spano, *J. Phys. Chem. C* **2016**, *120*, 11394.
[33] R. Ghosh, F. C. Spano, *Acc. Chem. Res.* **2020**, *53*, 2201.
[34] A. R. Chew, R. Ghosh, Z. Shang, F. C. Spano, A. Salleo, *J. Phys. Chem. Lett.* **2017**, *8*, 4974.
[35] D. T. Scholes, P. Y. Yee, J. R. Lindemuth, H. Kang, J. Onorato, R. Ghosh, C. K. Luscombe, F. C. Spano, S. H. Tolbert, B. J. Schwartz, *Adv. Funct. Mater.* **2017**, *27*, 1702654.

[36] T. J. Aubry, J. C. Axtell, V. M. Basile, K. J. Winchell, J. R. Lindemuth, T. M. Porter, J. Liu, A. N. Alexandrova, C. P. Kubiak, S. H. Tolbert, A. M. Spokoyny, B. J. Schwartz, *Adv. Mater.* **2019**, *31*, 1805647.
[37] R. Ghosh, A. R. Chew, J. Onorato, V. Pakhnyuk, C. K. Luscombe, A. Salleo, F. C. Spano, *J. Phys. Chem. C* **2018**, *122*, 18048.
[38] C. M. Pochas, F. C. Spano, *J. Chem. Phys.* **2014**, *140*, 244902.
[39] I. Sahalianov, J. Hynynen, S. Barlow, S. R. Marder, C. Müller, I. Zozoulenko, *J. Phys. Chem. B* **2020**, *124*, 11280.
[40] N. Zamoshchik, M. Bendikov, *Adv. Funct. Mater.* **2008**, *18*, 3377.
[41] N. Zamoshchik, U. Salzner, M. Bendikov, *J. Phys. Chem. C* **2008**, *112*, 8408.
[42] D. A. Stanfield, Y. Wu, S. H. Tolbert, B. J. Schwartz, *Chem. Mater.* **2021**, *33*, 2343.
[43] D. A. Stanfield, Z. Mehmedović, B. J. Schwartz, *Chem. Mater.* **2021**, *33*, 8489.
[44] E. C.-K. Wu, C. Z. Salamat, S. H. Tolbert, B. J. Schwartz, *ACS Appl. Mater. Interfaces* **2022**, *14*, 26988.
[45] G. Heimel, *ACS Cent. Sci.* **2016**, *2*, 309.
[46] Y. Yamashita, J. Tsurumi, M. Ohno, R. Fujimoto, S. Kumagai, T. Kurosawa, T. Okamoto, J. Takeya, S. Watanabe, *Nature* **2019**, *572*, 634.
[47] A. Hamidi-Sakr, L. Biniek, J.-L. Bantignies, D. Maurin, L. Herrmann, N. Leclerc, P. Lévêque, V. Vijayakumar, N. Zimmermann, M. Brinkmann, *Adv. Funct. Mater.* **2017**, *27*, 1700173.
[48] F. C. Spano, *J. Chem. Phys.* **2002**, *116*, 5877.
[49] F. C. Spano, *J. Chem. Phys.* **2005**, *122*, 234701.
[50] N. J. Hestand, F. C. Spano, *Chem. Rev.* **2018**, *118*, 7069.
[51] D. T. Scholes, P. Y. Yee, G. R. McKeown, S. Li, H. Kang, J. R. Lindemuth, X. Xia, S. C. King, D. S. Seferos, S. H. Tolbert, B. J. Schwartz, *Chem. Mater.* **2019**, *31*, 73.
[52] M. T. Fontana, D. A. Stanfield, D. T. Scholes, K. J. Winchell, S. H. Tolbert, B. J. Schwartz, *J. Phys. Chem. C* **2019**, *123*, 22711.
[53] L. Wu, H. Li, H. Chai, Q. Xu, Y. Chen, L. Chen, *ACS Appl. Electron. Mater.* **2021**, *3*, 1252.
[54] J. Yamamoto, Y. Furukawa, *J. Phys. Chem. B* **2015**, *119*, 4788.
[55] T. J. Aubry, K. J. Winchell, C. Z. Salamat, V. M. Basile, J. R. Lindemuth, J. M. Stauber, J. C. Axtell, R. M. Kubena, M. D. Phan, M. J. Bird, A. M. Spokoyny, S. H. Tolbert, B. J. Schwartz, *Adv. Funct. Mater.* **2020**, *30*, 2001800.
[56] N. Kayunkid, S. Uttiya, M. Brinkmann, *Macromolecules* **2010**, *43*, 4961.
[57] D. T. Scholes, S. A. Hawks, P. Y. Yee, H. Wu, J. R. Lindemuth, S. H. Tolbert, B. J. Schwartz, *J. Phys. Chem. Lett.* **2015**, *6*, 4786.
[58] N. Banerji, D. Tsokkou, P. Cavassin, G. Rebetez, O. Bardagot, in *Advances in Ultrafast Condensed Phase Physics III* (Eds.: V. Yakovlev, S. Haacke), SPIE, Strasbourg, France **2022**, p. 19.
[59] I. E. Jacobs, E. W. Aasen, J. L. Oliveira, T. N. Fonseca, J. D. Roehling, J. Li, G. Zhang, M. P. Augustine, M. Mascal, A. J. Moulé, *J. Mater. Chem. C* **2016**, *4*, 3454.
[60] C. Wang, Z. Zhang, S. Pejić, R. Li, M. Fukuto, L. Zhu, G. Sauvé, *Macromolecules* **2018**, *51*, 9368.
[61] Z. Jiang, *J. Appl. Crystallogr.* **2015**, *48*, 917.
[62] M. G. Voss, D. T. Scholes, J. R. Challa, B. J. Schwartz, *Farad. Disc.* **2019**, *216*, 339.